Taxis-driven pattern formation in a predator-prey model with group defense

Merlin C. Köhnke[a,*], Ivo Siekmann[b], Horst Malchow[a]

[a] *Institute of Mathematics, School of Mathematics/Computer Science, Osnabrück University, Germany*
[b] *Liverpool John Moores University, Department of Applied Mathematics, Liverpool, L3 3AF, England*

Abstract

We consider a reaction-diffusion(-taxis) predator-prey system with group defense in the prey. Taxis-driven instability can occur if the group defense influences the taxis rate (Wang et al., 2017). We elaborate that this mechanism is indeed possible but biologically unlikely to be responsible for pattern formation in such a system. Conversely, we show that patterns in excitable media such as **spatiotemporal** Sierpinski gasket patterns occur in the reaction-diffusion model as well as in the reaction-diffusion-taxis model. If group defense leads to a dome-shaped functional response, these patterns can have a rescue effect on the predator population in an invasion scenario. Preytaxis with prey repulsion at high prey densities can intensify this mechanism leading to taxis-induced persistence. In particular, taxis can increase parameter regimes of successful invasions and decrease minimum introduction areas necessary for a successful invasion. Last, we consider the mean period of the irregular oscillations. As a result of the underlying mechanism of the patterns, this period is two orders of magnitude smaller than the period in the nonspatial system. Counter-intuitively, faster-moving predators lead to lower oscillation periods and eventually to extinction of the predator population. The study does not only provide valuable insights on theoretical spatially explicit predator-prey models with group defense but also comparisons of ecological data with model simulations.

Keywords: predator invasion, group defense, reaction-diffusion, prey-taxis,

*Corresponding author
Email address: merlin.koehnke@uos.de (Merlin C. Köhnke)

July 5, 2020

pattern formation, excitable medium

1. Introduction

Systems of differential equations leading to oscillations are prevalent in a whole variety of ecological models and mathematical biology in general (Murray, 2002a). Relaxation oscillators are a particular type of oscillator that exhibit two different time scales. Many activator-inhibitor models are of this type if the activator time-scale is much shorter (Meron, 2015). Characteristic for such relaxation oscillators is the so-called excitement cycle: resting $\xrightarrow[\text{(slow)}]{\text{excitation}}$ excited $\xrightarrow[\text{(fast)}]{\text{relaxation}}$ resting (Ermentrout and Rinzel, 1981). With changes in parameters, this limit cycle can vanish via a homoclinic bifurcation. The resulting system is then called excitable (Ermentrout and Rinzel, 1981). Excitable means that perturbations above a threshold (super-threshold perturbations) lead to an excitation cycle, i.e., a relatively long excursion of the trajectory in the phase space. In contrast, a sub-threshold perturbation leads to direct convergence to the linearly stable equilibrium without such excitation behavior. Here, the excitation threshold is the stable manifold of the newly emerging saddle-node (Ermentrout and Rinzel, 1981; Kazantsev et al., 2003; Sevcikova and Marek, 1991).

Relaxation systems and systems with excitable kinetics are important for biological systems because they can lead to the formation of spatiotemporal patterns if the local kinetics are coupled with diffusive spread (Mendez et al., 2010). The spatially explicit dynamical system is then referred to as an excitable medium. It is well known that if the spatial domain is large enough, many patterns can emerge from a limit cycle in a nonspatial system also in systems without excitability (Conway et al., 1978). Examples for this are chaos in the wake of invasion (Sherratt et al., 1995), spiral waves (Keener and Tyson, 1986; Zaikin and Zhabotinsky, 1970), turbulence (Bär and Eiswirth, 1993), and target patterns (Stich and Mikhailov, 2006; Tyson and Fife, 1980). Experiments can reproduce such patterns (Irurzun et al., 2004; Lee et al., 1994; Marino and Balle, 2005). The triangle-shaped so-called Sierpinski gasket patterns give a particularly intriguing example (Hayase and Ohta, 2000; Kazantsev et al., 2003). **Note that in this manuscript as well as in the literature cited, Sierpinski gasket patterns refer to a spatiotemporal phenomenon whereas the classical Sierpinski triangle is a purely spatial pattern.** Even more intriguingly, these patterns

have indeed been observed in nature, for instance, on shell pigments (Lindsay, 1982; Meinhardt, 2009). They occur as a result of a combination of self-replicating pulses and different behavior occurring when pulses collide (Hayase, 1997). Self-replication denotes that a pulse splits into two pulses (Nishiura and Ueyama, 1999). If this pulse is traveling and the splitting pulse travels in the opposite direction, this phenomenon is denoted as backfiring (Mimura and Nagayama, 1997). Colliding pulses **are** only preserved under symmetric conditions (Hayase and Ohta, 2000). Such conditions are not possible with three existing pulses. In this case, annihilation occurs. Hence, every three pulse generations, the process repeats, and a pattern similar to Sierpinski gaskets emerges (Hayase and Ohta, 2000).

From an ecological perspective, it is essential to note that due to these patterns, the excitable nature of systems allows for persistent coexistence in spatially explicit systems that would otherwise not be possible. For instance, it can determine whether a biological invasion may be successful with potentially significant impacts on the whole ecosystem. Hence, it is essential to investigate such models in detail to understand diverse phenomena.

The dynamics in a classical pure reaction-diffusion system are well studied. With a classical pure reaction-diffusion system, we refer to a system in which the matrix of diffusion coefficients is diagonal, and the diagonal entries are constants. Ecologically this means that only the gradient of a species determines the dispersal of the same species. This assumption is strong in ecological contexts, and relaxing this assumption can significantly alter the outcome of spatiotemporal models. Recently, Zemskov et al. (2017) showed that cross-diffusion in a Bonhoeffer-van der Pol model could lead to solitary pulses or wave trains. Solitary pulses correspond to single traveling pulses representing a homoclinic solution, whereas the term wave train describes a sequence of such pulses (Zemskov et al., 2017). Roussel and Wang (2004) have analyzed a Gray-Scott model with variable diffusion coefficients showing **that** the resulting inhomogeneity in diffusivities can suppress self-replicating behavior. Furthermore, including advection in a model with Dirichlet boundary conditions can lead to the existence of wave trains (Vidal-Henriquez et al., 2017). In ecological contexts, already Shigesada et al. (1979) examined that movement responses to environmental potentials allow for spatial coexistence of competing populations due to spatial segregation. More recently, Potts and Petrovskii (2017) reported that incorporating taxis can also determine invasion success in a competitive system. A more common example of an ecological justification for the occurrence of a non-diagonal diffusion matrix

is given by preytaxis, i.e., the dependence of predator movement on the prey density gradient. Brindley et al. (2005) summarized impacts of pursuit-evasion dynamics, i.e., prey avoiding predators and predators attracted by prey, on biological invasions. Bate and Hilker (2019) investigated the impact of preytaxis on the speed of traveling waves. Furthermore, Lee et al. (2009) examined the impact of taxis on pattern formation. In particular, prey attraction tends to suppress Turing pattern formation. However, Wang et al. (2017) stated that prey repulsion can destabilize the spatial homogeneity of the system. A similar result was already obtained by Jorné (1977) for a Lotka-Volterra system with cross-diffusion if the prey moves towards higher predator densities. Wang et al. (2017) justified prey repulsion by group defense in the prey. However, the theoretical justification lacks investigation of whether such a situation occurs in a reasonable range of parameters in an ecological system. Furthermore, in general, the impact of non-diagonal matrices of diffusion coefficients in ecological systems (cross-diffusion) is not well studied yet compared to the classic reaction-diffusion case.

Here, we will consider an excitable predator-prey system with group defense in the prey. Following Wang et al. (2017), we will first discuss taxis-driven Turing instability, and with that, we will show that this is indeed possible for certain parameter combinations for our model. However, we will conclude that these parameter combinations do not make sense for a group defense predator-prey system. In Section 3.2, we will confirm that excitation patterns can emerge in this system. We will discuss in more detail how the spatial system influences the local period of oscillations. This is important as the period is a characteristic feature of oscillating systems and thus plays a role in comparison with experiments. Then, we show an example of how taxis can increase the parameter regime and the range of initial conditions allowing for such patterns. Finally, we will discuss the results.

2. Model and methods

We consider a spatially explicit predator-prey model

$$\frac{\partial U}{\partial T} = F_U(U,V) + D_U \Delta U,\ U(0,\vec{X}) = U_0(\vec{X}) \tag{1a}$$

$$\frac{\partial V}{\partial T} = F_V(U,V) + \nabla \cdot \sum_{i=1}^{2} \mathbf{J}_i,\ V(0,\vec{X}) = V_0(\vec{X}). \tag{1b}$$

Here, $\vec{X}$ is the position vector and $\Delta = \sum_{j=1}^{n} \frac{\partial^2 U}{\partial x_j^2}$ is the Laplace operator representing a randomly moving prey population. $\nabla \mathbf{J}_i$ is the divergence of the flux. Throughout this study, we will distinguish two different cases. In the first case, we assume that $i = 1$ and $\mathbf{J_1} = -D_V \nabla V$, i.e., diffusive flux with a constant diffusion coefficient D_V modeling movement of the predator population as well. In the second case, we consider $i = 2$ with $\mathbf{J}_2 = \tilde{\chi_0}\tilde{\chi}(U)V\nabla U$ additionally to the diffusive flux $\mathbf{J}_1$. This represents preytaxis with taxis rate $\tilde{\chi_0}\tilde{\chi}(U)$. Here, the predator movement is (partially) determined by the prey density gradient.

We assume a one-dimensional domain $[0, L]$, i.e., $j = 1$ throughout most of the study. Later on, we also use a square two-dimensional domain $j = 2$ for one simulation to visualize the patterns. To prevent boundary effects, we assume periodic boundary conditions

$$U(0) = U(L), \qquad U'(0) = U'(L), \tag{2a}$$
$$V(0) = V(L), \qquad V'(0) = V'(L). \tag{2b}$$

As we consider a predator-prey model with group defense in the prey, we use the kinetic equations developed in Köhnke et al. (2020)

$$F_U(U, V) = U(r - cU) - V\frac{\beta\gamma U}{\gamma + \beta U + \gamma(U/C)^\nu} \tag{3a}$$
$$F_V(U, V) = eV\frac{\beta\gamma U}{\gamma + \beta U + \gamma(U/C)^\nu} - mV \tag{3b}$$

with $\nu \geq 1$ and $C < rc^{-1}$. In a nutshell, the functional response has been derived by dividing the predator into handling and searching subpopulations of which only the searching subpopulation catches prey. These subpopulations are assumed to be in a quasi-steady state. The catch rate $g(U)$, in this case, is prey dependent and takes the form

$$g(U) = \frac{U}{1 + \left(\frac{U}{C}\right)^\nu}. \tag{4}$$

The prey grows logistically with growth rate r and intraspecific competition coefficient c. The predator dies linearly, with the mortality m. The rather complicated functional response represents group defense in the prey. In

particular, β is the search rate of the predator, and γ is the handling rate, i.e., the handling time is $H = \gamma^{-1}$. The parameters C and ν control the collective defense. ν controls the shape of the functional response. If $\nu = 1$, the functional response is saturating, whereas it is non-monotonic (or dome-shaped) if $\nu > 1$. Higher values of ν control how expressed the shape is. We will refer to it as the strength of the collective defense. C can be referred to as a critical defense value. It mainly affects the half-saturation density in the prey in case of saturation and the critical prey density at which the functional response has a maximum in case of a dome-shape. For a detailed explanation regarding the functional response and also the analysis of the nonspatial version of this model, we refer to Köhnke et al. (2020).

For convenience, the model can be nondimensionalized (see Appendix Appendix A for a description of all parameters and variables including their dimensions). Scaling the state variables $u = Ucr^{-1}$, $v = V\beta r^{-1}$, $x = X\left(D_U r^{-1}\right)^{-\frac{1}{2}}$, and $t = rT$, and introducing new parameters $\kappa = Cc(r)^{-1}$, $\alpha = \beta r(\gamma c)^{-1}$, $\mu = mr^{-1}$ $d = D_V D_U^{-1}$, $\chi_0 = r\tilde{\chi_0}(cD_U)^{-1}$ and $\epsilon = e\beta c^{-1}$ yields

$$\frac{\partial u}{\partial t} = u\left(1 - u - \frac{v}{1 + \alpha u + \left(u\kappa^{-1}\right)^{\nu}}\right) + \Delta u, u(0,x) = u_0(x), \tag{5a}$$

$$\frac{\partial v}{\partial t} = v\left(\frac{\epsilon u}{1 + \alpha u + \left(u\kappa^{-1}\right)^{\nu}} - \mu\right) + d\Delta v - \nabla \cdot \left(\chi_0 \chi(u) v \nabla u\right), \; v(0,x) = v_0(x). \tag{5b}$$

Throughout this study, only the defense parameters κ and ν as well as the ratio of diffusion coefficients d and the taxis rate $\chi_0\chi(u)$ have been varied. Table 1 lists the remaining parameters. They are based on a microtine rodent mustelid model from Hanski and Korpimäki (1995).

Table 1: The rescaled dimensionless parameters are shown with their value used throughout this study.

Parameter	**Value**
α	14.81
ϵ	5.06
μ	$2.47 \cdot 10^{-1}$

For the numerical treatment, we used a Strang splitting scheme as described in Bate and Hilker (2019) with a forward-time central-space scheme for the diffusion term, a fourth-order Runge-Kutta scheme for the reaction term, and an upwind method as described in Saito (2007) for the taxis term.

As initial conditions, we assume an invasion scenario. In particular, the predator invades a prey population. For the one-dimensional domain, the initial conditions are

$$v_0(x) = \left(\tanh\left(x-50\right) - \tanh\left(x-150\right)\right)\frac{\tilde{v}(\kappa)}{2} \tag{6a}$$

$$u_0(x) = 1 - \left(\tanh\left(x-50\right) - \tanh\left(x-150\right)\right)\frac{1-\tilde{u}(\kappa)}{2}. \tag{6b}$$

This is a continuous approximation of an invasion scenario in which the predator is introduced in the subinterval of the domain $x \in [50, 150]$ with density $\tilde{v}(\kappa)$, whereas the prey is at its carrying capacity in the rest of the domain. The values $\tilde{u}(\kappa) > 0$ and $\tilde{v}(\kappa) > 0$ are chosen such that they lie above the stable manifold of the nontrivial saddle point, see Figure 6 and corresponding text for further details.

3. Results

3.1. Taxis-driven instability

We start by considering Turing instabilities. In particular, we consider small heterogeneous perturbations $\delta_u(x,t)$ and $\delta_v(x,t)$ around the stationary coexistence state

$$u(x,t) = u_s + \delta_u(x,t), \qquad v(x,t) = v_s + \delta_v(x,t), \tag{7a}$$

$$\delta_u(x,t) = a_1 e^{\sigma t}\cos qx, \qquad \delta_v(x,t) = a_2 e^{\sigma t}\cos qx, \tag{7b}$$

see for instance Edelstein-Keshet (2005); Malchow et al. (2007). It is well known that independent of the form of the functional response developed above, diffusive instability leading to Turing patterns can never be possible as $Tr(J) < 0$ and $a_{11}D_2 + a_{22}D_1 > 0$ is not possible if $a_{22} = 0$ (Edelstein-Keshet, 2005; Fasani and Rinaldi, 2011). Note that pure preytaxis does also not have a destabilizing effect on a locally stable steady state (Lee et al., 2009). However, Wang et al. (2017) have shown that it may indeed be destabilizing

if the taxis-rate $\chi = \chi(u)$ is not constant. In this case, neglecting nonlinear perturbation terms, we get

$$\begin{pmatrix} \delta_u(x,t)_t \\ \delta_v(x,t)_t \end{pmatrix} = \begin{pmatrix} m_{11} & m_{12} \\ m_{21} & m_{22} \end{pmatrix} \begin{pmatrix} \delta_u(x,t) \\ \delta_v(x,t) \end{pmatrix} + \begin{pmatrix} 1 & 0 \\ -\chi_0\chi(u_s) & d \end{pmatrix} \begin{pmatrix} \delta_u(x,t)_{xx} \\ \delta_v(x,t)_{xx} \end{pmatrix} \quad (8)$$

for the temporal evolution of the perturbations. Here m_{ij} represents the entries of the Jacobian of the nonspatial version of Equation (5) evaluated at the stationary solution (u_s, v_s). Note that we assume, that $\chi(u)$ depends linearly on u and that we can thus neglect $\chi(\delta_u(x,t))\delta_v(x,t)_{xx}$. Inserting the perturbations, and neglecting the trivial case of $a_1 = a_2 = 0$ we get the characteristic equation

$$\sigma^2 - \psi_1\sigma + \psi_2 = 0 \quad (9)$$

with

$$\psi_1 = (m_{11} + m_{22} - (1+d)k)\,, \quad (10a)$$

$$\psi_2 = H(q^2) = dk^2 - k(m_{22} + dm_{11} + m_{12}v_s\chi_0\chi(u_s)) + m_{11}m_{22} - m_{12}m_{21}, \quad (10b)$$

where $k = q^2$. Equation (10a) is always negative in the spatial case if it is negative in the nonspatial case. Furthermore, as already stated in Wang et al. (2017), if $\chi_0\chi(u) > 0 \;\forall\; u$, taxis-driven instability is not possible as $m_{12} < 0$. However, taxis-driven instability can be possible if $\chi(u_s) < 0$. A justification for $\chi(u_s) < 0$ is group defense (Wang et al., 2017). In particular, the predator avoids areas in which the prey populations are at defending densities. Regarding the taxis rate, this means $\chi(u) > 0 \;\forall\; u < u_c$ and $\chi(u) < 0 \;\forall\; u > u_c$. A simple representation may be a linearly decreasing taxis rate

$$\chi(u) = 1 - \frac{u}{u_c}. \quad (11)$$

The **right** panel of Figure 1 shows a particular example of the emergence of spatiotemporal patterns due to preytaxis for such a given prey-dependent taxis rate. The **left** panel shows different combinations of κ and χ_0. It visualizes that low values of u_c and high values of χ_0 are necessary for taxis-driven instability. The colored region in Figure 2 shows the maximum value of u_c that can lead to taxis-driven instabilites — i.e., where negative values of Equation (10b) are possible — for different combinations of ν and κ.

However, in the following, we elaborate on why a taxis-driven instability is possible but not biologically meaningful in a collective defense model,

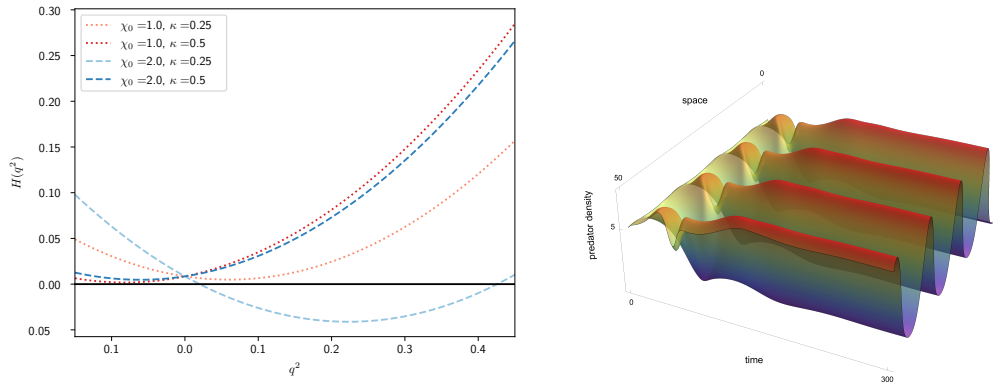

Figure 1: **Taxis-driven instability can occur if group defense leads to predator repulsion.** The **right** panel shows the emergence of taxis-driven instability for Equation (5) with parameters as stated in Table 1 and $\chi_0 = 2$. Note that only a part of the domain is shown for visualization. The taxis rate is assumed to be $\chi(u) = 1 - uu_c^{-1}$ with $u_c = \kappa = 0.25$. The **left** panel shows $H(q^2)$ as given by Equation (10b) for different values of u_c and χ_0.

as presented in this study. Recall that taxis-driven instability destabilizes a nonspatially stable stationary coexistence state. Such instability can only occur if $\chi(u_s) < 0$ (necessary). However, for an individual predator, repulsion from a high prey density does only make sense if $g'(u) < 0 \ \forall \ u > u_c$, i.e., if the catch rate is decreasing with higher prey densities. A necessary condition for the stability of the stationary coexistence state, however, is $g'(u_s) > 0$ corresponding to a positive determinant of the coexistence state (Köhnke et al., 2020). Hence, taxis-driven instability requiring $\chi(u_s) < 0$ is ecologically only meaningful for parameter combinations in which it is likely that $\chi(u_s) \geq 0$, which is a contradiction.

3.2. Patterns in excitable media

Apart from taxis-driven patterns, oscillatory patterns can arise due to the Hopf instability (Bär, 2019). In this section, we aim to investigate the potential impact of taxis on the occurrence of such patterns. Figure 2 shows in which parameter region of ν and κ representing the strength of group defense and its critical values, such patterns can occur. In the colored region, taxis-induced patterns can emerge as described in Section 3.1. In the nonspatial case, this region corresponds to stable stationary coexistence be-

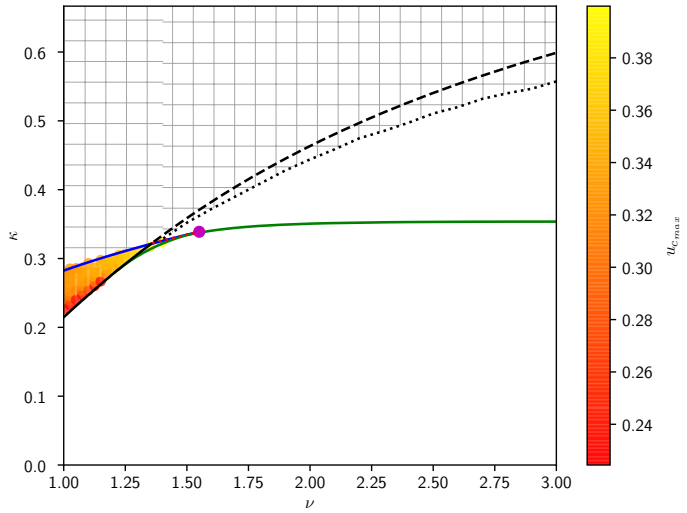

Figure 2: **Diffusion-induced oscillatory patterns can rescue the predator from extinction.** A two-dimensional bifurcation diagram of the critical defense value κ and the strength of the group defense ν is shown. The green line, blue, and solid black lines depict saddle-node, Hopf, and transcritical bifurcations, respectively. The black dashed line corresponds to a transcritical bifurcation and a homoclinic bifurcation, which co-occur. Below this curve, the predator goes extinct in the nonspatial case. In the spatial system, the predator persists in parameter regions until the dotted line (the hatched region) for some initial conditions. The color represents the maximum critical value u_c in Equation (11) that allows for taxis-induced pattern formation. The magenta dot represents a Bogdanov-Takens bifurcation point. Parameters are $d = 1$, $\chi_0 = 0$ except for the case of taxis-induced instability (colored region). Here, $d = 1$ and $\chi_0 = 2$. The remaining parameters are as stated in Table 1. We used XPPAUT (Ermentrout, 2002) for the computation of the nonspatial bifurcation curves and performed numerical simulations to calculate the colored regions and the dotted line.

tween predator and prey. Above this line and above the dashed black line, a limit cycle exists. This limit cycle vanishes due to a homoclinic bifurcation that co-occurs with a transcritical bifurcation. In the spatial system, the limit cycle turns into spatiotemporal patterns that persist until the dotted line in the whole hatched region. Hence, the diffusion (without taxis, i.e., $\chi_0 = 0$) rescues the predator from extinction in the parameter regime between the dotted and the dashed lines. Note that on the left-hand side of

the Bogdanov-Takens bifurcation point, bistability between the limit cycle and the prey-only state and between the stationary coexistence state and the prey-only state can emerge. However, this corresponds to a very limited region for this parameter set and is thus not further considered here. The interested reader is referred to Köhnke et al. (2020). Here, we want to focus on the emergence of the spatiotemporal patterns. In particular, Figure 2 shows that the emergence of patterns critically depends on the critical defense value κ. In the following, we will recall mechanisms of diffusion induced patterns in relaxation and excitable systems.

We start considering the emerging patterns for the case of a stable limit cycle. Figure 3 shows the spatiotemporal dynamics of Equation (5) without preytaxis. The predator population starts at a high density in the middle of the domain, whereas the prey is abundant all over the domain. The predator invasion takes place in the form of various traveling pulses leading to an intriguing triangle invasion shape. Such a triangle shape is often referred to as a Sierpinski gasket pattern (Hayase and Ohta, 2000; Kazantsev et al., 2003). It occurs due to self-replicating pulses and exists in diverse excitable systems (Hayase and Ohta, 2000). In particular, it emerges as preservation occurs for completely symmetric pulse collisions only, whereas non-symmetric pulse collisions lead to annihilation (Hayase and Ohta, 2000). However, note that such a triangle pattern can also be explained only focussing on the excitability of the system.

The slow-fast dynamics of the relaxation system govern the system dynamics. Here, the local dynamics between the carrying capacity and approximately the maximum of the limit cycle with respect to the predator correspond to the exciting (slow) process. In contrast, the local dynamics between the maximum and the origin correspond to the relaxation (fast) process in the relaxation system. Figure 4 shows the phase plane, including a vector field, and the limit cycle (black dashed lines) in panel a) for the nonspatial model. The magenta regions denote regions in the phase plane in which the trajectory of a point in space stays for relatively long times. In particular, the spatial trajectory roughly follows the limit cycle with a tendency to lower predator values due to the diffusive losses. The values were obtained numerically via a simulation of the one-dimensional system. They correspond to a particular point in space.

In the spatially explicit system, the diffusion acts as a perturbation from neighboring regions in space. This diffusive force is large compared to the low magnitude of the local rate of change close to the carrying capacity. Heuris-

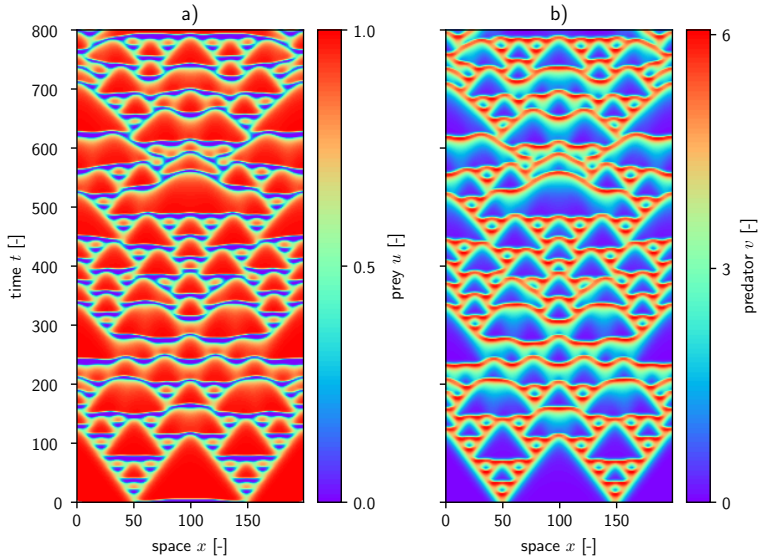

Figure 3: **Diffusion can lead to intriguing excitability patterns such as Sierpinski gasket patterns.** The spatiotemporal dynamics of Equation (5) with $j = 1$ is shown. The defense parameters are $\nu = 3$ and $\kappa = 0.67$. The diffusivities of the populations are equal, i.e., $d = 1$, while we do not consider preytaxis, i.e., $\chi_0 = 0$. The remaining parameters are as stated in Table 1.

tically speaking, the diffusive force of patches with initially high predator densities pushes the adjacent patches without predator to higher densities. Concurrently, the predator density of the patches with initially high predator densities shrinks due to the local dynamics and the diffusive losses. As this process repeats itself, it leads to propagating pulses in both directions, and a triangle shape emerges. If such pulses meet, the neighboring area is already excited, and hence, the pulse cannot propagate any further (Meinhardt and Klingler, 1987). The larger triangles emerge if neighboring areas in the excited state become larger due to several pulses meeting at the same time. In this case, the excitation wave can only propagate outwards. This excitation wave represents the initial wave (Meinhardt and Klingler, 1987). Note that the local dynamics must be slow enough to observe a rather distinct triangle pattern.

In our case, the Sierpinski gasket pattern is distorted due to two different reasons. First, the initially large predator patch leads to two initial pulses

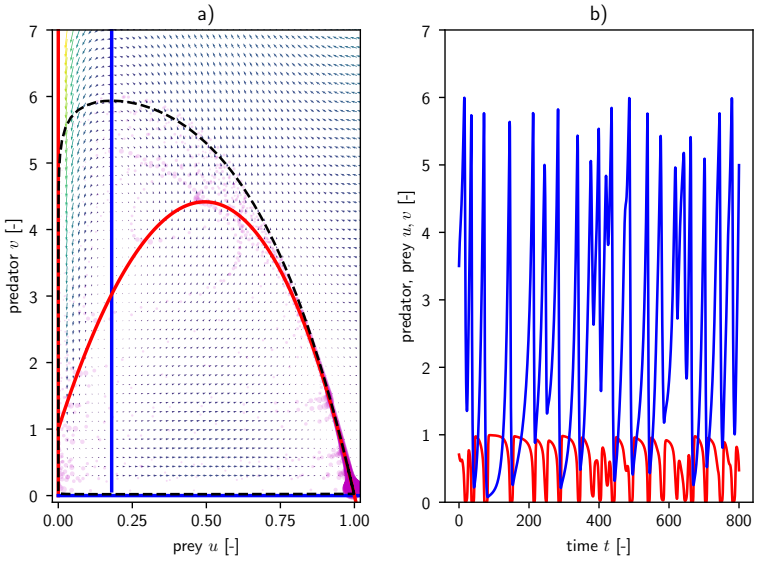

Figure 4: **Phase plane analysis, including spatial trajectories indicates that the slow-fast dynamics of the system drive the emerging patterns.** In both panels, red lines correspond to the prey, whereas blue lines correspond to the predator (nullclines in panel a) and solutions at one spatial point in b)). Panel a) shows a phase portrait with a vector field for the nonspatial model. The dashed line shows the limit cycle. Magenta regions correspond to regions in which the spatial system at one particular point in space stays for relatively long times. Panel b) shows the time series corresponding to the magenta regions. The magenta regions and the time series were calculated for a particular point in space. The parameters are as stated in Figure 3.

at the border of the initially occupied patches. When the invasion waves resulting from these separate pulses meet, the clear Sierpinski gasket pattern gets destroyed. Second, the large triangles with very low predator densities get blurry probably as a result of the local dynamics which are not negligibly small on this time scale anymore. As a result of these perturbations, locally, these oscillations appear irregular, as shown in panel b) of Figure 4.

Figure 5 shows an example of these spatiotemporal patterns for a parameter combination that leads to extinction of the predator in the nonspatial model in two dimensions. In this case, the relaxation system has become excitable as the stable limit cycle has been destroyed via a homoclinic bifurcation. The predator spreads via pulsating circles visible at $t = 250$ and $t = 500$. This propagation directly translates to a spatiotemporal pattern

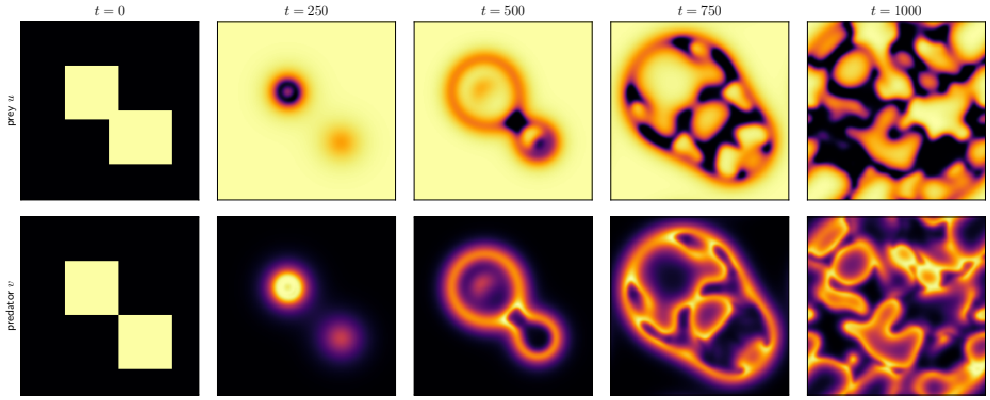

Figure 5: **Nonsymmetrical initial conditions can lead to irregular spatiotemporal patterns.** The spatial configuration for prey (upper row) and predator (lower row) is shown. Lighter colors correspond to higher densities. Parameters are such that the carrying capacity is the only stable stationary solution in the nonspatial model. In particular, $d = 1$, $\kappa = 0.57$, $\chi_0 = 0$, and $\nu = 3$. The remaining parameters are as stated in Table 1.

similar to the one in Figure 3, although it is less regular due to the different initial conditions. Conversely to the classical excitation pulse (Müller, 2019), the propagation of the excitation happens not only in one direction, but the area behind the excited state becomes excitable quickly again. This so-called wave splitting occurs if the diffusion is sufficiently strong to excite the wake of the wave (Petrov et al., 1994). Experiments have reproduced such a phenomenon (Manz and Steinbock, 2006). In the present system, it is primarily due to the fast dynamics behind the upper cluster in Figure 4. In the final configuration, it is apparent that the prey is abundant at high densities over parts of the domain, whereas the predator is mainly abundant at distinct lines. Furthermore, some parts exist in which neither prey nor predator is abundant. This is consistent with the magenta regions in Figure 4. The system stays in the neighborhood of the two (semi-)trivial equilibria due to the slow local dynamics, but also at coexistence regions close to the maximum of the nontrivial prey nullcline.

It is known that traveling pulses in excitable systems exhibit a strong dependence on initial conditions (Murray, 2002b). In particular, the stable manifold of the saddle gives the excitation threshold (Ermentrout and Rinzel, 1981; Kazantsev et al., 2003; Sevcikova and Marek, 1991). The right panel of Figure 6 shows the dependence of pattern formation on the initial conditions

in the present system. This dependence is particularly relevant in an invasion scenario. The initial conditions need to start above the stable manifold.

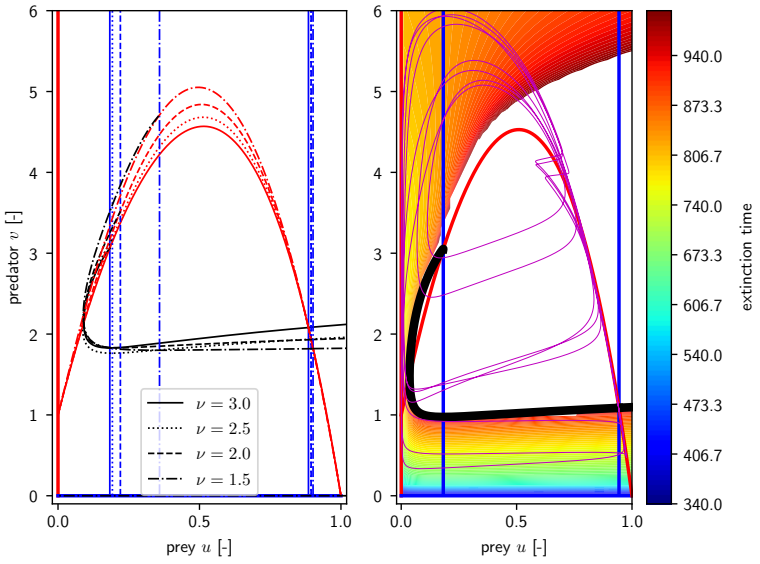

Figure 6: **The dependence of the rescue effect on the stable manifold leads to a strong dependence on initial conditions for invasion scenarios.** The left panel shows phase portraits for different values of ν. In particular, it is shown how the nontrivial nullclines and the stable manifold of the saddle (right coexistence solution) change with respect to ν. The extinction time, i.e., the time until the carrying capacity is reached, is color-coded. In the white area, the predator does not go extinct in the spatiotemporal model. The magenta line shows a trajectory at one particular point in space. Colors are as in Figure 4. The parameters are as in Figure 5.

Starting above the stable manifold allows the system to converge to the capacity via the unstable manifold of the saddle which has a form similar to the limit cycle. Hence, the system passes through high predator densities, and the mechanism takes place as described before. Thus, in an invasion scenario, the predator needs to be introduced at sufficiently high densities to ensure its survival.

However, this is necessary but not sufficient because if the initial predator population densities are too high, the predator goes extinct. Starting at very high predator densities, the local dynamics becomes too fast (cf. vector field in Figure 4), and the system would converge to the prey **carrying** capacity

(and thus below the excitation threshold) too quickly.

Keeping in mind that the stable manifold is a separatrix, we look at the phase space configuration for the lowest value of κ for which patterns emerge for a given ν (cf. dotted line in Figure 2). The left panel of Figure 6 visualizes the results. This value seems to be predominantly driven by the right predator nullcline, as this is the same (accounting for numerical uncertainties) for all values of ν. If the right nullcline is shifted further to the left with lower values of C, numerical simulations indicate that the threshold is too high for excitability via the diffusive force. In other words, the diffusion cannot push the spatial areas that are close to the carrying capacity in the phase portrait over the stable manifold of the saddle-node. Note that this does not depend on the magnitude of the diffusion coefficient but on the predator density in the wake of the invasion wave and the spatial extent of the wake. If the spatial extent and/or the density is too small/low, the predator goes extinct before it can excite the neighboring areas. Numerical simulations with other parameter combinations, in particular different diffusion coefficients, suggest that this is indeed the underlying mechanism.

It is known, that the spatiotemporal dynamics in excitable systems can lead to spatially triangular, but temporally irregular patterns (Kazantsev et al., 2003). Although it is also known that the local oscillation period is shorter in a perturbed excitable system, the exact impact is not well investigated (Crucifix, 2012). **In the nonspatial system, the period of the limit cycle diverges approaching the homoclinic bifurcation (see red line in Figure 7).** In the spatial system the mean period also increases with decreasing κ, cf. blue dots in the left panel of Figure 7. We calculated the mean period as the mean of periods over all spatial grid cells. In turn, we calculated the mean of each spatial grid cell as the mean periods over a time interval $t \in [1000, 10000]$ to neglect transient behavior. The spatial period is two orders of magnitude smaller than in the nonspatial case. For comparisons of model simulations with ecological time series, the period is an important indicator. As ecological systems are naturally spatially explicit, it is essential to know that diffusion in relaxation systems can reduce the period significantly. The reason is that the diffusion shortens the excitation time, which is mainly contributing the most to the length of the period. Furthermore, interestingly, the period has a local maximum at the homoclinic bifurcation ($\kappa \gtrapprox 0.6$) as the dynamics shortly before the homoclinic orbit becomes very slow. However, this effect is not very prominent.

As the mechanism given suggests that the period is short, particularly

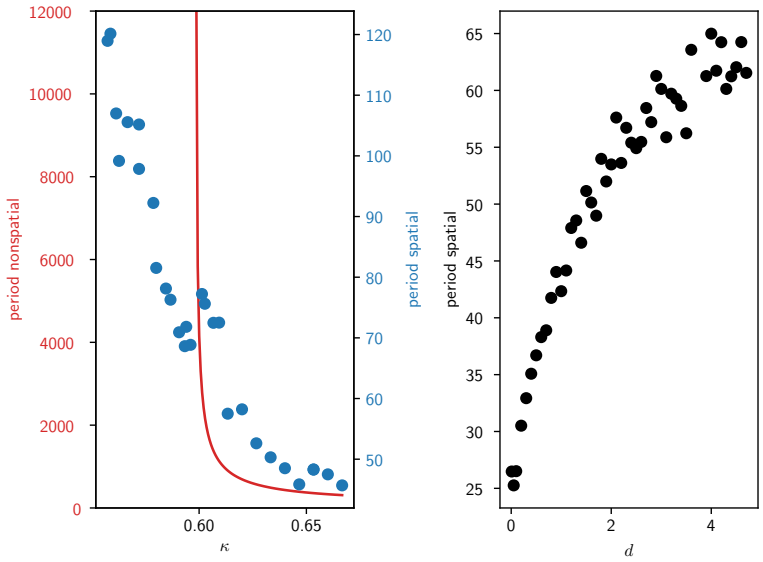

Figure 7: **Diffusion shortens the oscillation period by two orders of magnitude.** The period of the oscillations is shown for the nonspatial model (red) and the spatial model (blue). In the nonspatial model, the period diverges when it approaches the homoclinic bifurcation. Conversely, the period increases beyond this bifurcation point in the spatial model. The right panel shows that this is rather independent of the value of d as the order of magnitude is the same. However, the ratio of diffusivities also influences the period (see text for further details). Parameters are as in Figure 5 for the spatial model and as in Figure 4 in the nonspatial model. For the right panel, $\kappa = 0.59$ is assumed.

due to the movement of the predator populations, we also show the impact of different ratios of predator/prey diffusivities. In the right panel of Figure 7, it is shown that the period increases with higher values of d. This is counter-intuitive at first glance as one could assume that higher predator dispersal enhances the rescuing effect and decreases the period. However, as already mentioned, the rescue effect depends strongly on the extent of the predator patches. With higher diffusivity, approximately the same population spreads over a larger area. Hence, for an individual cell, the rescue effect is smaller, and the period becomes longer. As the patch sizes with high predator densities do not change with respect to d, this effect is saturating. If d becomes larger, the rescue effect becomes even impossible.

Ecologically, this is counter-intuitive as higher movement abilities are

usually assumed to correspond to higher invasion abilities. Hence, we showed that for relaxation systems, this could indeed be the other way round.

3.3. Preytaxis in excitable media

Recall that the lowest κ allowing for spatiotemporal patterns is determined by the stable manifold of the saddle-node. With this, we can now investigate the impact of taxis. In particular, we consider two different cases apart from the diffusion-only case, which are sketched in Figure 8.

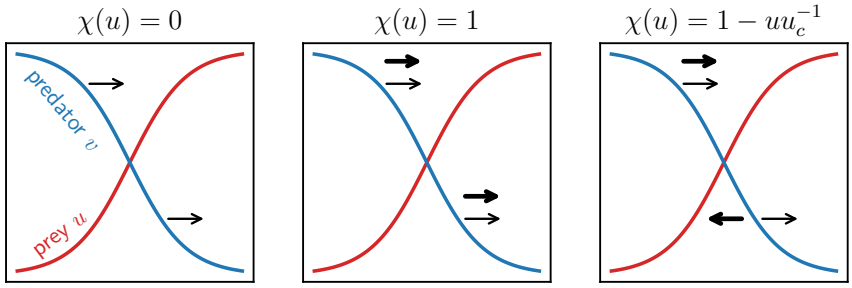

Figure 8: **The influence of taxis depends on the form of the taxis rate.** The sketch of the impact of three different forms of the taxis rate $\chi(u)$ are shown. The left panel shows the case with only diffusive flux denoted by thin arrows. The middle panel shows a case with preytaxis and diffusion and the right panel shows a case with Equation (11) as taxis rate and diffusion.

The left panel shows a pure diffusion case with $\chi_0 = 0$. The thin arrows denote the direction of the diffusive flux down the predator gradient. Considering preytaxis, in a typical situation, this flux is even enhanced, see the middle patch of Figure 8. The diffusive flux denoted by the thin arrows stays as before, but the tactic flux indicated by the thick arrows enhances the overall flux. A typical situation means that the sign of the gradient of the predator density is opposite to the sign of the gradient of the prey density. If pure diffusion does not allow for pattern formation, the additional tactic flux does not change that. The reason is that the predator density in the wake will spread over a larger area, making it impossible to push neighboring spatial areas over the excitation threshold. The right panel refers to a tactic flux representing predator movement response to group defense. At low prey densities, the predator moves up the prey density gradient. However, at high prey densities, the predator tries to avoid the prey and moves down the prey gradient. Here, taxis-driven pattern formation can occur. Figure 9

shows such a situation in which, in **the** absence of taxis, the predator would go extinct. The magenta regions denote regions in which the prey is below

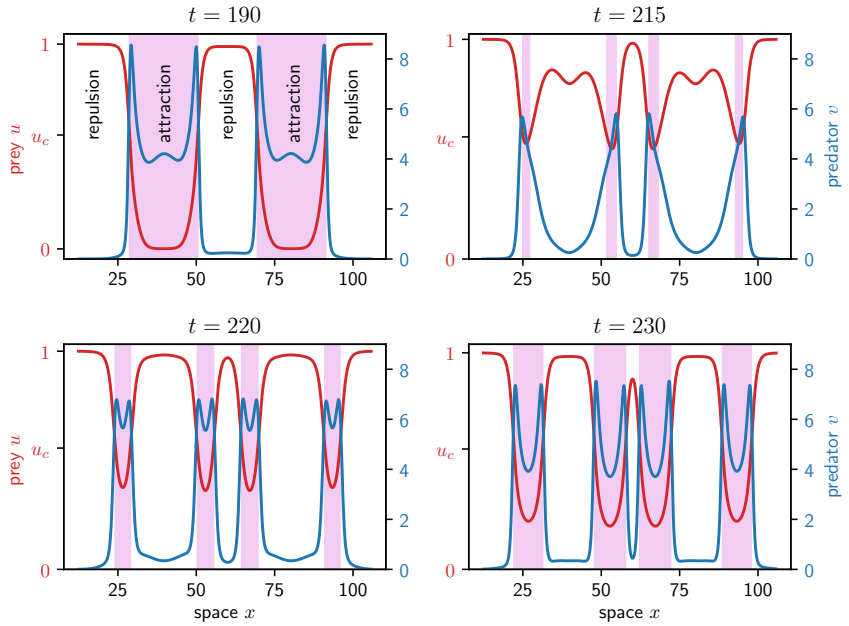

Figure 9: **Taxis can lead to a successful predator invasion.** Snapshots at different time steps for the same spatial region are shown. The taxis rate is given by Equation (11) with $\chi_0 = 7$, $u_c = \kappa$, and $d = 0.4$. The remaining parameters are as in Figure 5.

the critical density and thus, the predator would move the prey gradient upwards. The prey repulsion happens mainly in regions in which the predator is only at low densities. This increases the predator density at the peak of the leading edge, cf. upper left panel. Due to that, the predator is still at high densities when the prey converges to its carrying capacity in the neighboring areas again, cf. upper right panel. From this state, the predator can perturb the adjacent regions to excite the system again, cf. lower left panel. From here, the excitation cycle can start again, cf. lower right panel. Without taxis, the predator would have spread faster to the regions of high prey densities in the upper panels. Due to that, the predator densities would have been too low to excite the adjacent regions again.

This taxis-driven pattern formation can have two different effects. First, it can increase the values of κ allowing for pattern formation. However,

this depends on the magnitude of the taxis and the critical value u_c. In particular, if the value is too high, the effect would be too low. Conversely, if the value is too low, the predator would just tend to aggregate. Second, it allows for smaller initial predator patches that lead to a successful invasion visualized by Figure 10. In particular, with a high taxis rate, the minimum

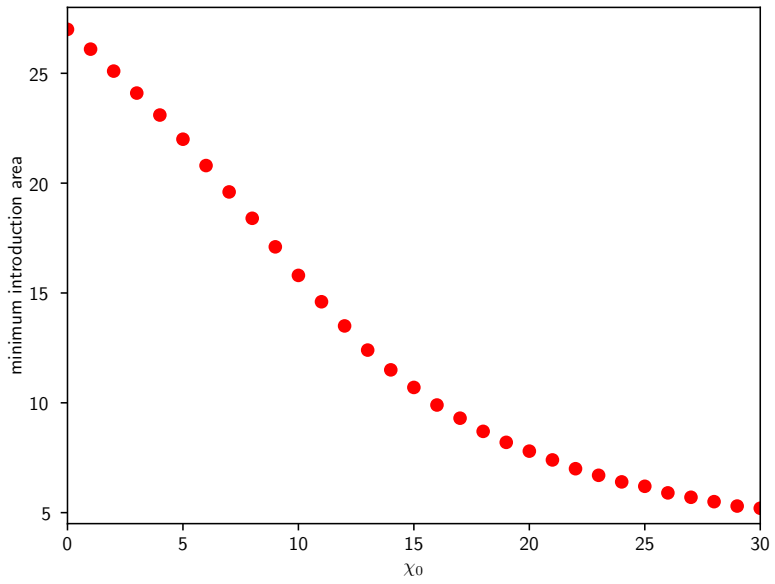

Figure 10: **Critical introduction areas necessary for successful spread can become smaller with higher taxis rates.** The initially occupied area necessary for a successful predator establishment is shown depending on the magnitude of the taxis. Taxis rate is given by Equation (11) with varying χ_0, $u_c = \kappa$, and $d = 0.4$. The remaining parameters are as in Figure 5.

introduction area necessary for a successful invasion is more than five times lower. The reason for this relation is also the 'effective use' of the predator peaks, as described above. However, the impact seems to be saturating with high taxis rates. This may be due to **the fact** that with high χ_0, the prey attraction coupled with the diffusive motion is already too high even though they only occur at densities below u_c. Due to this, specific neighboring areas cannot become excited, and the predator goes extinct quickly. On the other hand, the saturating effect can also simply be reducible to the

fact that negative areas are not possible. Hence, the minimum introduction areas must converge to values greater than or equal to zero for high taxis rates. Independent of the exact mechanism, this is an important finding from an invasion perspective because particularly the initial phases introduction, reproduction, and survival are critical states in determining invasion success (Blackburn et al., 2011).

4. Discussion and Conclusion

In this study, we extended the predator-prey model incorporating group defense proposed in Köhnke et al. (2020) by spatial spread. Wang et al. (2017) have shown that taxis-driven instability can occur in such a system if group defense is present. Although we find the same conditions for taxis-driven instability and provide numerical examples for it, we challenge the hypothesis that such patterns can occur in group defense predator-prey models. In particular, we have shown that for the model considered in this study, such a phenomenon can only occur if the predator movement is not ecologically optimal.

In contrast, we have shown that excitability patterns may indeed emerge if the homogeneous system has a limit cycle. As the amplitude of the limit cycle can be very high corresponding to temporary low population densities, such spatial patterns can be interpreted as a rescue effect (Brown and Kodric-Brown, 1977) as they may increase the resilience of the system against environmental perturbations. However, note that spatially synchronized external forcings, such as the weather, can synchronize the oscillations again if they are large enough (Liebhold et al., 2004). Furthermore, it is well known that coupled oscillators in experiments can synchronize their phase, a phenomenon known as phase locking (Marek and Stuchl, 1975; Murray, 2002a).

The spatiotemporal patterns also sustain beyond the homoclinic bifurcation that is destroying the limit cycle in the nonspatial system. This phenomenon is well known for relaxation oscillators that become excitable media after the vanishing of the limit cycle. We have proposed evidence showing that the underlying mechanism for the patterns is indeed given by the diffusive force coupled with the slow and fast dynamics in the nonspatial system (Müller, 2019). In this case, the limit cycle vanishes via a homoclinic bifurcation. With bifurcation analysis, we have shown that this effect only occurs for $\nu > 1$ corresponding to a dome-shaped functional response. This is a phenomenon that is not possible in the system with a simple saturating

functional response as it relies on the existence of two nontrivial stationary solutions. Hence, this can be interpreted as a defense-induced phenomenon. However, note that also a saturating functional response can represent group defense if a critical prey density does not exist, see Köhnke et al. (2020) for further details.

Furthermore, we refer to the spatiotemporal patterns as invasion patterns as they strongly depend on initial conditions that may correspond to an invasion scenario. This is also a known feature of such excitable systems (Murray, 2002b). In our case, the predator as the invader needs to be absent in some regions but present in the other regions at sufficiently high densities. In particular, we have shown the importance of the stable manifold of the saddle-node for the existence of such patterns. First, the initial conditions must lie over the stable manifold, and second, the stable manifold needs to be sufficiently low such that the diffusion can push the system beyond it. Furthermore, if the predator is above the excitation threshold all over the domain, the diffusive rescue effect cannot take place even if one applies small perturbations to the initial conditions. Already Ermentrout and Rinzel (1981) report the criticality of the stable manifold of the saddle as a perturbation threshold. However, the specific region allowing for spatial patterns also depends on the vector field of the local system. In particular, we have shown that initial conditions that are too high lead to the extinction of the predator.

Moreover, we considered the mean period of the rather irregular spatial oscillations at each point in space. Counter-intuitively, higher predator motility increases the mean period and can eventually suppress the rescue effect. Generally, the period is two orders of magnitude lower than the regular oscillations in the nonspatial system. This is due to the diffusive perturbations decreasing the time the system spends in the destabilizing region of the phase plane close to the prey carrying capacity. Note that including environmental noise in models with relaxation dynamics has the same effect based on the same mechanism (Crucifix, 2012). As most natural systems may indeed include space, movement, and environmental perturbations, this makes a comparison of ecological time series with model simulations challenging. This is because ecological time series are often measured at a particular point in space, and the period is a crucial feature of such a time series. Thus, if the considered system shows slow-fast dynamics, a spatial component is necessary for a reliable comparison.

Numerical simulations indicate that the minimum critical defense value

allowing for such spatiotemporal patterns is driven by the configuration of the nullclines and the stable manifold of the saddle that is destroying the limit cycle. Keeping this mechanism in mind, we investigated the effect of preytaxis. In particular, we have shown that preytaxis representing avoidance of large prey groups can extend the parameter regime corresponding to a rescue effect even further. In terms of a biological invasion of the predator, the initial (introduced) predator patch size leading to a successful establishment of the predator can be significantly smaller than without preytaxis.

Note that for the simulations performed in this study, the excitability patterns remained non-stationary in space and time for all the simulation time. However, Petrov et al. (1994) reported that steady wave interaction could lead to wave locking and accompanying stationary patterns in the long run. Even with extensive simulations, we did not find such a scenario. However, this would depend on a combination of simulation time and the size of the domain and may still exist for some combinations.

Finally, we want to emphasize that the main aim of this study was to identify possible impacts of taxis on the occurrence of spatiotemporal patterns in a group defense predator-prey model. Although we question that Turing patterns are driven by taxis in a group defense setting, excitability patterns can at least partly occur due to taxis. Hence, like various other studies in the field of population dynamics (e.g., Bate and Hilker, 2019; Potts and Petrovskii, 2017; Shigesada et al., 1979), this suggests that the impact of not only self-diffusive movement should get broader attention in future research.

Appendix A. Dimensions

Table A.2 summarizes the meaning of the parameters and state variables including their dimensions.

Table A.2: The dimensions of the parameters and state variables as used in Equation (1) as well as their biological meaning are shown with T, N, and L representing dimensions of time, population size, and length respectively. Here, we assume one spatial dimension.

	Meaning	**Dimension**
U	prey	N
V	predator	N
T	time	T
X	space	L
r	prey growth rate	T^{-1}
c	prey competition coefficient	$(\mathrm{TN})^{-1}$
β	search rate of the predator	$(\mathrm{TN})^{-1}$
γ	handling rate	T^{-1}
C	critical defense value	N
ν	strength of collective defense	-
e	conversion efficiency	-
m	predator mortality	T^{-1}
D_U	prey diffusion coefficient	$\mathrm{L}^2\mathrm{T}^{-1}$
D_V	predator diffusion coefficient	$\mathrm{L}^2\mathrm{T}^{-1}$
$\tilde{\chi_0}$	prey taxis coefficient	$\mathrm{L}^2(\mathrm{NT})^{-1}$

References

Bär, M. (2019). Reaction-diffusion patterns and waves: From chemical reactions to cardiac arrhythmias. In *Spirals and Vortices*, pages 239–251. Springer.

Bär, M. and Eiswirth, M. (1993). Turbulence due to spiral breakup in a continuous excitable medium. *Physical Review E*, 48(3):R1635.

Bate, A. M. and Hilker, F. M. (2019). Preytaxis and travelling waves in an eco-epidemiological model. *Bulletin of Mathematical Biology*, 81(4):995–1030.

Blackburn, T. M., Pyšek, P., Bacher, S., Carlton, J. T., Duncan, R. P., Jarošík, V., Wilson, J. R., and Richardson, D. M. (2011). A proposed unified framework for biological invasions. *Trends in Ecology & Evolution*, 26(7):333–339.

Brindley, J., Biktashev, V., and Tsyganov, M. (2005). Invasion waves in populations with excitable dynamics. *Biological Invasions*, 7(5):807–816.

Brown, J. H. and Kodric-Brown, A. (1977). Turnover rates in insular biogeography: effect of immigration on extinction. *Ecology*, 58(2):445–449.

Conway, E., Hoff, D., and Smoller, J. (1978). Large time behavior of solutions of systems of nonlinear reaction-diffusion equations. *SIAM Journal on Applied Mathematics*, 35(1):1–16.

Crucifix, M. (2012). Oscillators and relaxation phenomena in Pleistocene climate theory. *Philosophical Transactions of the Royal Society A: Mathematical, Physical and Engineering Sciences*, 370(1962):1140–1165.

Edelstein-Keshet, L. (2005). *Mathematical models in biology*. SIAM.

Ermentrout, B. (2002). *Simulating, analyzing, and animating dynamical systems: a guide to XPPAUT for researchers and students*, volume 14. Siam.

Ermentrout, G. B. and Rinzel, J. (1981). Waves in a simple, excitable or oscillatory, reaction-diffusion model. *Journal of Mathematical Biology*, 11(3):269–294.

Fasani, S. and Rinaldi, S. (2011). Factors promoting or inhibiting turing instability in spatially extended prey–predator systems. *Ecological Modelling*, 222(18):3449–3452.

Hanski, I. and Korpimäki, E. (1995). Microtine rodent dynamics in northern europe: parameterized models for the predator-prey interaction. *Ecology*, 76(3):840–850.

Hayase, Y. (1997). Collision and self-replication of pulses in a reaction diffusion system. *Journal of the Physical Society of Japan*, 66(9):2584–2587.

Hayase, Y. and Ohta, T. (2000). Self-replicating pulses and Sierpinski gaskets in excitable media. *Physical Review E*, 62(5):5998.

Irurzun, I., Imbihl, R., Vicente, J., and Mola, E. (2004). An analysis of turbulent states in the NH3 + NO reaction on Pt {1 0 0}. *Chemical Physics Letters*, 389(1-3):212–217.

Jorné, J. (1977). The diffusive lotka-volterra oscillating system. *Journal of Theoretical Biology*, 65(1):133–139.

Kazantsev, V., Nekorkin, V., Binczak, S., and Bilbault, J. (2003). Spiking patterns emerging from wave instabilities in a one-dimensional neural lattice. *Physical Review E*, 68(1):017201.

Keener, J. P. and Tyson, J. J. (1986). Spiral waves in the Belousov-Zhabotinskii reaction. *Physica D: Nonlinear Phenomena*, 21(2-3):307–324.

Köhnke, M. C., Siekmann, I., Seno, H., and Malchow, H. (2020). A type IV functional response with different shapes in a predator-prey model. *Manuscript submitted for publication*.

Lee, J., Hillen, T., and Lewis, M. (2009). Pattern formation in prey-taxis systems. *Journal of Biological Dynamics*, 3(6):551–573.

Lee, K.-J., McCormick, W. D., Pearson, J. E., and Swinney, H. L. (1994). Experimental observation of self-replicating spots in a reaction–diffusion system. *Nature*, 369(6477):215–218.

Liebhold, A., Koenig, W. D., and Bjørnstad, O. N. (2004). Spatial synchrony in population dynamics. *Annu. Rev. Ecol. Evol. Syst.*, 35:467–490.

Lindsay, D. T. (1982). A new programmatic basis for shell pigment patterns in the bivalve mollusc *Lioconcha castrensis* (l.). *Differentiation*, 21(1-3):32–36.

Malchow, H., Petrovskii, S. V., and Venturino, E. (2007). *Spatiotemporal patterns in ecology and epidemiology: theory, models, and simulation*. CRC Press.

Manz, N. and Steinbock, O. (2006). Propagation failures, breathing pulses, and backfiring in an excitable reaction-diffusion system. *Chaos: An Interdisciplinary Journal of Nonlinear Science*, 16(3):037112.

Marek, M. and Stuchl, I. (1975). Synchronization in two interacting oscillatory systems. *Biophysical Chemistry*, 3(3):241–248.

Marino, F. and Balle, S. (2005). Excitable optical waves in semiconductor microcavities. *Physical Review Letters*, 94(9):094101.

Meinhardt, H. (2009). *The algorithmic beauty of sea shells*. Springer Science & Business Media.

Meinhardt, H. and Klingler, M. (1987). A model for pattern formation on the shells of molluscs. *Journal of Theoretical Biology*, 126(1):63–89.

Mendez, V., Fedotov, S., and Horsthemke, W. (2010). *Reaction-transport systems: mesoscopic foundations, fronts, and spatial instabilities*. Springer Science & Business Media.

Meron, E. (2015). *Nonlinear physics of ecosystems*. CRC Press.

Mimura, M. and Nagayama, M. (1997). Nonannihilation dynamics in an exothermic reaction-diffusion system with mono-stable excitability. *Chaos: An Interdisciplinary Journal of Nonlinear Science*, 7(4):817–826.

Müller, S. C. (2019). Generation of spirals in excitable media. In *Spirals and Vortices*, pages 141–155. Springer.

Murray, J. D. (2002a). *Mathematical biology I: An introduction*. Springer, 3rd edition.

Murray, J. D. (2002b). *Mathematical biology II: Spatial models and biomedical applications*. Springer, 3rd edition.

590 Nishiura, Y. and Ueyama, D. (1999). A skeleton structure of self-replicating
591 dynamics. *Physica D: Nonlinear Phenomena*, 130(1-2):73–104.

592 Petrov, V., Scott, S. K., and Showalter, K. (1994). Excitability, wave reflec-
593 tion, and wave splitting in a cubic autocatalysis reaction-diffusion system.
594 *Philosophical Transactions of the Royal Society of London. Series A: Phys-*
595 *ical and Engineering Sciences*, 347(1685):631–642.

596 Potts, J. R. and Petrovskii, S. V. (2017). Fortune favours the brave: Move-
597 ment responses shape demographic dynamics in strongly competing pop-
598 ulations. *Journal of Theoretical Biology*, 420:190–199.

599 Roussel, M. R. and Wang, J. (2004). Pattern formation in excitable me-
600 dia with concentration-dependent diffusivities. *The Journal of Chemical*
601 *Physics*, 120(17):8079–8088.

602 Saito, N. (2007). Conservative upwind finite-element method for a simplified
603 Keller–Segel system modelling chemotaxis. *IMA Journal of Numerical*
604 *Analysis*, 27(2):332–365.

605 Sevcikova, H. and Marek, M. (1991). Wave patterns in an excitable reaction-
606 diffusion system. *Physica D: Nonlinear Phenomena*, 49(1-2):114–124.

607 Sherratt, J. A., Lewis, M. A., and Fowler, A. C. (1995). Ecological chaos
608 in the wake of invasion. *Proceedings of the National Academy of Sciences*,
609 92(7):2524–2528.

610 Shigesada, N., Kawasaki, K., and Teramoto, E. (1979). Spatial segregation
611 of interacting species. *Journal of Theoretical Biology*, 79(1):83–99.

612 Stich, M. and Mikhailov, A. S. (2006). Target patterns in two-dimensional
613 heterogeneous oscillatory reaction–diffusion systems. *Physica D: Nonlinear*
614 *Phenomena*, 215(1):38–45.

615 Tyson, J. J. and Fife, P. C. (1980). Target patterns in a realistic model
616 of the Belousov–Zhabotinskii reaction. *The Journal of Chemical Physics*,
617 73(5):2224–2237.

618 Vidal-Henriquez, E., Zykov, V., Bodenschatz, E., and Gholami, A. (2017).
619 Convective instability and boundary driven oscillations in a reaction-
620 diffusion-advection model. *Chaos: An Interdisciplinary Journal of Non-*
621 *linear Science*, 27(10):103110.

Wang, Q., Song, Y., and Shao, L. (2017). Nonconstant positive steady states and pattern formation of 1D prey-taxis systems. *Journal of Nonlinear Science*, 27(1):71–97.

Zaikin, A. and Zhabotinsky, A. (1970). Concentration wave propagation in two-dimensional liquid-phase self-oscillating system. *Nature*, 225(5232):535–537.

Zemskov, E. P., Tsyganov, M. A., and Horsthemke, W. (2017). Oscillatory pulses and wave trains in a bistable reaction-diffusion system with cross diffusion. *Physical Review E*, 95(1):012203.